Correspondence

Pseudo-Zernike Moments Based Sparse Representations for SAR Image Classification

We propose radar image classification via pseudo-Zernike moments based sparse representations. We exploit invariance properties of pseudo-Zernike moments to augment redundancy in the sparsity representative dictionary by introducing auxiliary atoms. We employ complex radar signatures. We prove the validity of our proposed methods on the publicly available moving and stationary target acquisition and recognition dataset.

I. INTRODUCTION

Synthetic aperture radar (SAR) can provide all-weather imagery with a very high resolution [1]. This has naturally led to using SAR for the purpose of automatic target recognition or classification. The initial usage was military related. However, SAR imaging with the aim of classification is making very quick strides for the automotive usage as well [2]. Traditionally, a number of techniques are used for SAR image classification. A state-of-the-art review on different approaches used for automatic target recognition in SAR imagery can be found in [3]. Here, we briefly mention a couple of them. Template-based classification [4] requires generation of a large number of templates for each target and then matching the test image with those templates in an exhaustive search manner. It is an effective linear approach. However, it is computationally quite expensive. Among the nonlinear approaches, support vector machine classifier (SVC) has been quite popular [5]. It is a large margin classifier and can outperform the template-based classifier. However, this approach is dependent upon the accurate estimation of the pose angle, which involves an extra preprocessing stage.

Recent trends in classification are based on sparse representations, also known as sparse coding [6], [7]. Initially, efforts were made to find or use a unified dictionary for all the classes, see, e.g., [8], [9], and the references therein. Instead of using a single dictionary for all the classes, Wright *et al.* [10] proposed to use unit-normalized measurements of the objects as the columns of an overcomplete dictionary.

Manuscript received April 10, 2018; revised July 10, 2018; released for publication July 10, 2018. Date of publication July 16, 2018; date of current version April 11, 2019.

DOI. No. 10.1109/TAES.2018.2856321

Refereeing of this contribution was handled by L. Rosenberg.

This work was supported in part by the Jaguar Land Rover and in part by the UK-EPSRC under Grant EP/N012240/1 as part of the jointly funded Towards Autonomy: Smart and Connected Control Programme.

Authors' address: S. Gishkori and B. Mulgrew are with the Institute for Digital Communications, School of Engineering, The University of Edinburgh, Edinburgh EH9 3JL, U.K., E-mail: (s.gishkori@ed.ac.uk; bernie.mulgrew@ed.ac.uk). *(Corresponding author: Shahzad Gishkori.)*

Coding is done through an ℓ_1-norm minimization problem and the classification is based on a least-squares metric w.r.t. the group of columns specific to a particular class object. This is known as sparse representation based classifier (SRC). The ease of formulating a dictionary by using the measurements of the class objects directly made SRC a favorable choice for classification in a wide range of fields. In SAR image classification, SRC was used in [11] from the perspective of class manifolds [12]. A class manifold is defined over the set of measurements for a particular class object, and the SAR image is claimed to lie in that manifold by using the fact that linear representation can be provided to a nonlinear manifold if a local region of the manifold is considered [13]. This local region of the manifold gives the basis for sparse representation of a test image over that manifold. Therefore, it obviates the need for a rigorous preprocessing as well as pose-angle estimation. Dimensionality reduction can be achieved via random projections. However, it can result in a performance loss.

It was shown in [10] and [11] that SRC can outperform linear SVC (LSVC), i.e., when a linear kernel is used. However, SRC is primarily based upon sparse reconstruction or coding, and it does not involve the classification aspect during the coding process. A number of papers have been written to incorporate this aspect in sparse representations. Some discriminative dictionary learning techniques have been proposed in [14] and [15]. Similarly, joint dictionary learning and encoding has been proposed in [16] (see, e.g., [17] and [18] for such recent attempts). Although these methods provide good performance but dictionary learning, whether discriminative or not, is a computationally intensive process.

Moments based image representations have been successfully used over many decades [19], [20]. The basic idea is to derive image features, which are scale-, shift-, and rotation-invariant by using nonlinear combinations of the regular moments (also called geometric moments). However, the gains have been limited, primarily due to the nonorthogonality of regular moments. Orthogonal moments, e.g., Legendre moments, Zernike moments, and pseudo-Zernike (PZ) moments [21], [22] have been a popular substitute in pattern recognition. Among these, PZ moments stand apart both in terms of generating the maximum number of invariant moments and in terms of performance regarding noise rejection. PZ moments have been used for radar automatic target recognition in [23] with a nearest neighbor classifier. Similarly, in [24], PZ moments have been used for radar classification based on its micro-Doppler signatures, with an SVC. However, in both these cases, the emphasis has been on feature extraction w.r.t. PZ moments and not on the choice of an optimal classifier.

Contributions: In this paper, we propose using PZ moments in combination with the SRC framework (PZ-SRC), in order to gain from both optimal feature extraction and optimal classification. By using a finite number of PZ moments, we reduce the dimensionality of the problem. This has a direct impact on reducing the computational complexity of the proposed method, as shown in subsequent sections. Due to invariance properties of the PZ moments, we obtain good performance, albeit in the low-dimensional setting. We also introduce auxiliary atoms in the dictionary to increase the redundancy of information, which further exploits the invariance properties of the PZ moments. Thus, information is better localized in individual class manifolds. This results in a further improvement in classification performance. Note, this also forms a unique contribution to the SRC framework, in general, as well. In order to utilize both the magnitude and the phase information of the complex radar signatures, we fuse the two parameters by a simple averaging mechanism (see [25] for details on the fusion mechanisms). This results in even more informative radar signatures with direct positive impact over the classification performance. Note, a similar approach has been used in [26]. However, the feature extraction there is based on regular moments and the authors do not use auxiliary atoms. Now, in order to encode the test image in our proposed framework of PZ-SRC, we use the state-of-the-art technique of iterative hard thresholding (IHT) algorithm [27]. IHT provides very fast convergence as well accuracy (in comparison with the approach in [10]), both of which are crucial in real-time radar image classification applications. We test our proposed methods on the publicly available moving and stationary target acquisition and recognition (MSTAR) dataset [28].

Organization: Section II gives the basics of PZ moments, Section III briefly describes the SRC method, Section IV details our proposed method of PZ-SRC, Section V provides experimental results, and conclusions are given in Section VI.

Notations: Matrices are in upper case bold whereas column vectors are in lower case bold, $(\cdot)^T$ denotes transpose, $[\mathbf{x}]_i$ is the ith element of $\mathbf{x}$, $\hat{\mathbf{x}}$ is the estimate of $\mathbf{x}$, $\triangleq$ defines an entity, and the ℓ_p-norm is denoted as $||\mathbf{x}||_p = (\sum_{i=0}^{N-1} |[\mathbf{x}]_i|^p)^{1/p}$.

II. PZ MOMENTS

Let a piecewise continuous function $s(x, y)$ (with bounded support) be the intensity function of a two-dimensional real image in Cartesian coordinates. The regular moments of $s(x, y)$ can be defined as

$$\mu_{p,q} = \int_x \int_y x^p y^q s(x, y)\, dx\, dy \tag{1}$$

where $\{p, q\} \in \mathbb{Z}_+$ and $p + q$ is the degree of the moments. Note, (1) represents the projection of $s(x, y)$ on monomial $x^p y^q$. Since $\{x^p y^q\}$ is not an orthogonal set, $\mu_{p,q}$ are not independent moments. In contrast, the PZ moments are generated from a set of orthogonal polynomials. We refer to these polynomials as PZ polynomials. The PZ polynomials are a set of complex polynomials described as

$$z_n^m(r, \theta) = \rho_n^m(r) \exp(jm\theta) \tag{2}$$

where $r \triangleq \sqrt{x^2 + y^2}$ and $\theta \triangleq \tan^{-1}(y/x)$ are the length and angle of the position vector of a point (x, y) w.r.t. the center of the image, respectively, $n \in \mathbb{Z}_+$ is the degree of

the polynomial with frequency m, i.e., $m \in [-n, +n]$, and

$$\rho_n^m(r) \triangleq \sum_{\kappa=0}^{n-|m|} \frac{(-1)^\kappa\,(2n+1-\kappa)!\,r^{n-\kappa}}{\kappa!\,(n+|m|+1-\kappa)!\,(n-|m|-\kappa)!} \quad (3)$$

is the radial polynomial. When defined over a unite circle, i.e., $r \leq 1$, the PZ polynomials exhibit orthogonality, i.e.,

$$\int_0^{2\pi}\int_0^1 [z_n^m(r,\theta)]^* z_{n'}^{m'}(r,\theta)\,r\,dr\,d\theta = \frac{\pi}{n+1}\delta_{nn'}\delta_{mm'} \quad (4)$$

where $\delta_{ii'}$ is the Kronecker delta function. Note, it can be seen via simple enumeration that cardinality of the set of PZ polynomials with degree $\leq n$ is $P = (n+1)^2$. Now, the PZ moments can be obtained by projecting the image onto the PZ polynomials as[1]

$$a_n^m = \frac{n+1}{\pi}\int_0^{2\pi}\int_0^1 [z_n^m(r,\theta)]^* s(r,\theta)\,r\,dr\,d\theta \quad (5)$$

where $s(r,\theta) = s(x,y)|_{x=r\cos\theta, y=r\sin\theta}$. Due to (4), it can be shown that (5) generates a set of independent moments.

The invariance properties of the PZ moments can be established via mathematical manipulations. For scale and translation invariance, one way is to use the regular moments of the image. The transformed image can be written as

$$g(x,y) = s\left(\frac{x}{\upsilon} + m_x, \frac{y}{\upsilon} + m_y\right) \quad (6)$$

where $m_x \triangleq \mu_{1,0}/\mu_{0,0}$ and $m_y \triangleq \mu_{0,1}/\mu_{0,0}$ are the centroid adjustment parameters of the image $s(x,y)$, and $\upsilon \triangleq \sqrt{\xi/\mu_{0,0}}$ is the scale adjustment parameter of the image $s(x,y)$ with a predetermined value ξ. Now, the scale- and translation-invariant PZ moments can be generated by replacing $s(r,\theta)$ with $g(r,\theta)$ in (5), where $g(r,\theta) = g(x,y)|_{x=r\cos\theta, y=r\sin\theta}$. Since PZ polynomials are a set of complex polynomials, the PZ moments generated via (5) are also complex. The rotation invariance of the PZ moments refers to the magnitude part only, i.e., $|a_n^m|$ and not the phase.

III. SPARSE REPRESENTATION BASED CLASSIFIER

Let a generic $\sqrt{N}\times\sqrt{N}$ image with intensity function $g(x,y)$ or $g(r,\theta)$ is represented as an $N\times 1$ vector $\mathbf{g}$ via a lexicographic ordering (column or row ordered). Let $\mathbf{g}_j^k$ be the jth image measurement of the kth object class, for $j = 1,\ldots,J_k$ and $k = 1,\ldots,K$. Now, given a set of training image measurements $\{\mathbf{g}_j^k\}$, with $\|\mathbf{g}_j^k\|_2^2 = 1$, the SRC method defines the dictionary as

$$\mathbf{G} \triangleq [\mathbf{G}^1, \mathbf{G}^2, \ldots, \mathbf{G}^K] \quad (7)$$

where $\mathbf{G}$ is an $N\times J$ matrix with $J = \sum_{k=1}^K J_k$ and $\mathbf{G}^k \triangleq [\mathbf{g}_1^k, \mathbf{g}_2^k, \ldots, \mathbf{g}_{J_k}^k]$ is an $N\times J_k$ matrix acting as a sub-dictionary for class k, for $k = 1,\ldots,K$. Any test image measurement, represented as an $N\times 1$ vector $\tilde{\mathbf{y}}$ can then be decomposed or encoded according to the linear model

$$\tilde{\mathbf{y}} = \mathbf{G}\tilde{\mathbf{x}} + \tilde{\mathbf{n}} \quad (8)$$

where $\tilde{\mathbf{x}}$ is a $J\times 1$ vector of coefficients defined as, $\tilde{\mathbf{x}} \triangleq [\tilde{\mathbf{x}}^{1\,T}, \tilde{\mathbf{x}}^{2\,T}, \ldots, \tilde{\mathbf{x}}^{K\,T}]^T$, where $\tilde{\mathbf{x}}^k$ are the coefficients w.r.t. the submatrix $\mathbf{G}^k$, and the $N\times 1$ vector $\tilde{\mathbf{n}}$ accounts for model errors with a bounded energy, i.e., $\|\tilde{\mathbf{n}}\|_2 < \tilde{\epsilon}$. It is clear from (8) that given $\tilde{\mathbf{y}}$ belongs to the kth class, $\tilde{\mathbf{x}}$ would be a sparse vector. Now, an estimate of $\tilde{\mathbf{x}}$ can be obtained by solving the following ℓ_1-norm optimization problem (OP):

$$\hat{\tilde{\mathbf{x}}} = \arg\min_{\tilde{\mathbf{x}}} \|\tilde{\mathbf{y}} - \mathbf{G}\tilde{\mathbf{x}}\|_2^2 + \lambda\,\|\tilde{\mathbf{x}}\|_1^1 \quad (9)$$

where $\lambda > 0$. The classification result is then obtained by finding k for which $\|\tilde{\mathbf{y}} - \mathbf{G}^k\hat{\tilde{\mathbf{x}}}^k\|_2^2$ is minimum, for $k = 1,\ldots,K$. In case of the feature based representation, the SRC model takes the form

$$\mathbf{R}\tilde{\mathbf{y}} = \mathbf{R}\mathbf{G}\tilde{\mathbf{x}} + \mathbf{R}\tilde{\mathbf{n}} \quad (10)$$

where $\mathbf{R}$ is an $R\times N$ linear transformation matrix. When $R < N$, it can reduce the computational complexity of the SRC approach. However, it may reduce the classification performance as well. If the elements of $\mathbf{R}$ are drawn from a normal/Gaussian distribution, i.e., $\mathcal{N}(0,1)$, (10) is known as SRC with random projections (R_ω-SRC) [11], where $R = N/\omega$ and $\omega \geq 1$.

IV. PZ MOMENTS BASED SPARSE REPRESENTATIONS

In this paper, we consider feature based sparse representations. In our case, PZ moments form the feature set of the radar image. Since PZ moments are generated by projecting the image onto PZ polynomials, we can easily generate the features by converting the PZ polynomials into a basis matrix and then projecting the image vector onto this basis matrix.

Let a $P\times 1$ vector $\mathbf{z}_i$ of PZ polynomials, with degree $\leq n$, w.r.t. image point (r_i,θ_i), where (r_i,θ_i) are the polar coordinates equivalent of the image point (x_i, y_i) in Cartesian coordinates, for $i = 1,\ldots,N$, be defined as

$$\begin{aligned}\mathbf{z}_i \triangleq [&\gamma_0 z_0^0(r_i,\theta_i), \gamma_1 z_1^{-1}(r_i,\theta_i), \gamma_1 z_1^0(r_i,\theta_i), \gamma_1 z_1^{+1}(r_i,\theta_i)\\ &\ldots, \gamma_n z_n^{-n}(r_i,\theta_i), \gamma_n z_n^{-n+1}(r_i,\theta_i), \ldots, \gamma_n z_n^{+n}(r_i,\theta_i)]^T\end{aligned} \quad (11)$$

where $\gamma_n \triangleq (n+1)/(\pi N)$ accounts for subsequent constants as well as integration to summation approximations in (5). Note, we assume that $r_i \leq 1 \quad \forall i \in [1, N]$, which ensures that all image points are within the unit circle. The PZ polynomials based basis matrix can then be defined as a $P\times N$ matrix $\mathbf{Z}$, i.e.,

$$\mathbf{Z} \triangleq [\mathbf{z}_1, \mathbf{z}_2, \ldots, \mathbf{z}_N] \quad (12)$$

which is still a matrix of complex polynomials. Now, given a set of training image measurements $\{\mathbf{g}_j^k\}$, for $j = 1,\ldots,J_k$ and $k = 1,\ldots,K$, the dictionary based on PZ moments features, with the property of rotational invariance, can be defined as a column normalized (i.e., normalized to unity)

[1]Note, in case of a digital image, the integrals in the projection operations are replaced by summations.

$P \times J$ matrix $\mathbf{A}$, i.e.,

$$\mathbf{A} \triangleq \text{abs}\left(\mathbf{ZG}\right) = \left[\mathbf{A}^1, \mathbf{A}^2, \ldots, \mathbf{A}^K\right] \tag{13}$$

where abs$(\cdot)$ is a function that generates elementwise absolute values, and $\mathbf{A}^k \triangleq \text{abs}\left(\mathbf{ZG}^k\right)$ is a $P \times J_k$ matrix of PZ moments w.r.t. $\mathbf{G}^k$, for $k = 1, \ldots, K$. In order to capitalize on the invariance structure provided by PZ moments, we introduce auxiliary atoms in the dictionary (see Section IV-B). Thus, the dictionary can be defined as

$$\begin{aligned}\mathbf{\Phi} &\triangleq \left[\left[\mathbf{A}^1, f\left(\mathbf{A}^1\right)\right], \left[\mathbf{A}^2, f\left(\mathbf{A}^2\right)\right], \ldots, \left[\mathbf{A}^K, f\left(\mathbf{A}^K\right)\right]\right] \\ &= \left[\mathbf{\Phi}^1, \mathbf{\Phi}^2, \ldots, \mathbf{\Phi}^K\right]\end{aligned} \tag{14}$$

where $f(\mathbf{A}^k)$ is a $P \times L_k$ auxiliary matrix (with columns normalized to unity) and it is a function of the columns of $\mathbf{A}^k$, $\mathbf{\Phi}^k \triangleq [\mathbf{A}^k, f(\mathbf{A}^k)]$ is a $P \times Q_k$ matrix with $Q_k = J_k + L_k$, for $k = 1, \ldots, K$, and the overcomplete dictionary $\mathbf{\Phi}$ is a $P \times Q$ matrix with $Q = \sum_{k=1}^{K} Q_k$. Now, the test image $\tilde{\mathbf{y}}$ can be encoded according to the following linear model:

$$\mathbf{y} = \mathbf{\Phi x} + \mathbf{n} \tag{15}$$

where $\mathbf{y} \triangleq \text{abs}(\mathbf{Z}\tilde{\mathbf{y}})$ is the $P \times 1$ vector of PZ moments of the test image, $\mathbf{x}$ is the $Q \times 1$ encoded vector defined as, $\mathbf{x} \triangleq [\mathbf{x}^{1\,T}, \mathbf{x}^{2\,T}, \ldots, \mathbf{x}^{K\,T}]^T$, where $\mathbf{x}^k$ is the $Q_k \times 1$ encoding vector w.r.t. $\mathbf{\Phi}^k$, for $k = 1, \ldots, K$, and $\mathbf{n}$ is the $P \times 1$ model error vector with bounded energy, i.e., $\|\mathbf{n}\|_2 < \epsilon$. It is clear from (15), given that the test image belongs to a particular class, $\mathbf{x}$ would be a sparse vector with nonzero elements ideally corresponding to the subdictionary of only a particular class.

A. Sparse Reconstruction and Classification

Since $P \ll Q$, (15) is an underdetermined system of linear equations. In order to recover $\mathbf{x}$ in (15), we use IHT as the sparse recovery algorithm. An estimate of $\mathbf{x}$ can be obtained by processing the following iterations:

$$\hat{\mathbf{x}}^{[t+1]} = \mathcal{H}_\Gamma\left(\hat{\mathbf{x}}^{[t]} + \mathbf{\Phi}^T\left(\mathbf{y} - \mathbf{\Phi}\hat{\mathbf{x}}^{[t]}\right)\right) \tag{16}$$

where t is the iteration index (starting with $t = 0$) and $\mathcal{H}_\Gamma$ is the hard thresholding operator defined as

$$\mathcal{H}_\Gamma(\mathbf{q}) \triangleq \mathbf{q}\mathbb{I}_{\{i \,|\, [\mathbf{q}]_i \geq [\text{Ascend}(\mathbf{q})]_\Gamma,\, \forall i\}} \tag{17}$$

where $\mathbb{I}_{\{\cdot\}}$ is an indicator operatorthat discards those elements of vector $\mathbf{q}$ that are not in the indicator set (the set given in its subscript), and Ascend$(\mathbf{q})$ is a sorting function that sorts the elements of $\mathbf{q}$ in an ascending order. Essentially, $\mathcal{H}_\Gamma(\mathbf{q})$ preserves only the Γ largest element magnitudes of $\mathbf{q}$ in each iteration t. Thus, (16) approximates the ℓ_0-norm estimate of $\mathbf{x}$, i.e.,

$$\hat{\mathbf{x}} = \arg\min_{\mathbf{x}} \|\mathbf{y} - \mathbf{\Phi x}\|_2^2 \quad \text{subject to} \;\; \|\mathbf{x}\|_0^0 \leq \Gamma \tag{18}$$

where Γ is the order of sparsity. Note, the stopping criterion of iterations in (16) can either be the maximum number of allowable iterations or the minimum residual error, i.e., $\|\mathbf{y} - \mathbf{\Phi}\hat{\mathbf{x}}^{[t]}\|_2^2 / \|\mathbf{y}\|_2^2$. After sparse encoding of $\mathbf{y}$, the classification of the target image can be done by solving the following OP:

$$\hat{k} = \arg\min_k \left\|\mathbf{y} - \mathbf{\Phi}^k\hat{\mathbf{x}}^k\right\|_2^2, \quad \text{for } k = 1, \ldots, K \tag{19}$$

where $\hat{\mathbf{x}}^k$ is the estimate obtained in the PZ-SRC framework, when the stopping criterion for (18) has been achieved.

Note, the computational complexity of IHT for PZ-SRC is $\mathcal{O}(PQ)$ per iteration, where $\mathcal{O}(\cdot)$ denotes the order of complexity. Since $P \ll N$, the computational complexity of PZ-SRC is much lower than that of the SRC.

B. Auxiliary Atoms

The auxiliary atoms can have a substantial impact on the performance of the classification. Ideally, variations in the image measurements w.r.t. different aspect angles should not produce any variations in their respective PZ moments. However, radar reflectivities at different aspect angles might not be uniform. Therefore, an image at one aspect angle might be absolutely different from the image obtained at another aspect angle. Also, noise in the form of clutter or other artifacts can play a disruptive role. Auxiliary atoms try to recover the information lost due to these irregularities. In this section, we present a number of techniques to generate the auxiliary atoms. Note, here our focus is primarily on rotational invariance of the moments.

1) *Fixed Auxiliary Atoms (AuxFix):* In case the measurements are obtained at random aspect angles, we propose to constitute the auxiliary atoms as an overall average of the PZ-moments based measurements of each class, i.e.,

$$f(\mathbf{A}^k) = \sum_{j=1}^{J_k} \mathbf{a}_j^k \tag{20}$$

where $\mathbf{a}_j^k \triangleq \text{abs}(\mathbf{Zg}_j^k)$, for $k = 1, \ldots, K$. AuxFix causes the effect of irregular reflectivities to be averaged out. Here, $L_k = 1$, for $k = 1, \ldots, K$.

2) *Moving-Average Based Auxiliary Atoms (AuxMov):* In case the measurements are arranged in the order of increasing aspect angles around the object, a moving average of atoms over each class can constitute the auxiliary atoms, i.e.,

$$f_j(\mathbf{A}^k) \;\; = \sum_{w=-W_k/2}^{+W_k/2} \mathbf{a}_{w+j}^k \tag{21}$$

where W_k is the window size for the kth class, for $k = 1, \ldots, K$, and $j = 1, \ldots, J_k$. We can see that the window is centered over the jth column of $\mathbf{A}^k$. Note, in case $(w + j) < 1$ or $(w + j) > J_k$, $\mathbf{a}_{w+j}^k$ can be considered as zero vectors. Here, $L_k = J_k$. The auxiliary matrix can be formed as

$$f(\mathbf{A}^k) = \left[f_1(\mathbf{A}^k), f_2(\mathbf{A}^k), \ldots, f_{J_k}(\mathbf{A}^k)\right]. \tag{22}$$

3) *Correlation Based Auxiliary Atoms (AuxCorr):* An optimal method is to find correlated atoms w.r.t. every training measurement for each class, i.e., the columns of $\mathbf{A}^k$. The auxiliary atoms can then be generated based on a minimum

correlation value, i.e.,

$$f_j(\mathbf{a}^k) = \sum_{\substack{l=1 \\ a_j^{k\,T}\mathbf{a}_l^k > \Upsilon}}^{J_k} \mathbf{a}_l^k \tag{23}$$

where $\mathbf{a}_j^{k\,T}\mathbf{a}_l^k$ performs the inner product, Υ is the correlation threshold, and $j = 1, \ldots, J_k$. Here, $L_k = J_k$. The auxiliary matrix can be formed according to (22). This procedure ensures that all informative measurements, i.e., measurements with high mutual correlation, are accounted for.

C. Complex Signatures

We can see from the previous sections that most of the classification strategies use only the intensities or magnitudes of the images. However, a radar signature contains information both in the magnitude and the phase. One way to benefit from both sources of information is to create an image of the target scene from each of these sources and then use an image fusion technique to optimally combine them into a single fused image. This resulting image will have more information of the target scene than the magnitude-only and the phase-only images. To this end, we combine the magnitude and the phase of the radar signatures via an averaging fusion mechanism, and use the fused image to create the PZ moments. Thus, the fused image has the generalized form, $\alpha[\log(\text{abs}(\{\mathbf{g}_j^k\}))] + \beta[\text{phase}(\{\mathbf{g}_j^k\})]$, where phase$(\cdot)$ is an elementwise phase-generating function, and, $0 < \alpha \leq 1$ and $0 < \beta \leq 1$ denote the magnitude and phase fractions, respectively. Note, we use an averaging fusion mechanism due to the ease of its implementation and the generality of its applicability across all classes of the target objects. However, other image fusion techniques, optimal for each target class (based on different performance metrics), can also be used to further enhance the classification performance. See [25] for more details on different image fusion techniques.

V. EXPERIMENTAL RESULTS

In this section, we present experimental results of our proposed methods. We use the publicly available MSTAR dataset. The MSTAR data were collected by Sandia National Laboratory by using an X-band SAR (in spotlight mode) with 1-ft resolution. We consider three targets from this dataset, i.e., 2S1 tank, D-7 land clearing vehicle, and T62 tank (so $K = 3$). Fig. 1 shows the optical and SAR (magnitude only) images for one aspect angle of these targets.

For the purpose of training, a total of $J_k = 299$ measurements are considered, for each target, at a radar elevation angle of 17°. The measurements have been taken at sequentially increasing aspect angles of approximately 1.2°, i.e., covering the complete angular range of 360°. Note, the measurements are in the form of 96×96 SAR images. These images are vectorized for the sake of processing. Thus, $N = 9216$. For the purpose of testing, a total of 273 image measurements (for each class) are considered, which have been taken at different aspect angles over the complete angular range of 360°, with a radar elevation angle of 15°. Aspect angles of the testing measurements are different from the training measurements. Thus, pose-angle estimation is a valid issue. We define the classification/recognition accuracy/performance for the kth class as

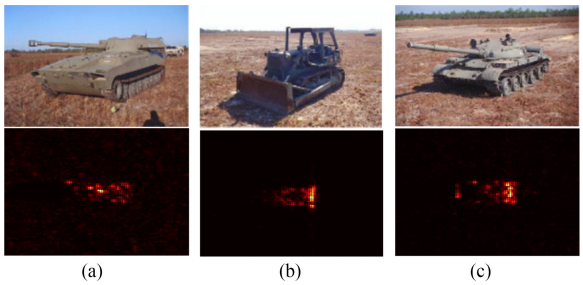

Fig. 1. MSTAR targets. (a) 2S1. (b) D-7. (c) T62.

TABLE I
Performance Comparison of Different Classifiers

	$\Omega_1(\%)$	$\Omega_2(\%)$	$\Omega_3(\%)$	$\Omega(\%)$
LSVC	91.94	98.90	92.67	94.50
PZ-LSVC	93.40	99.26	96.33	96.33
SRC	95.97	99.26	93.04	96.09
R_{05}-SRC	95.97	99.26	92.31	95.24
R_{15}-SRC	95.24	98.53	90.84	94.87
R_{35}-SRC	92.67	98.53	88.64	93.28
PZ-SRC	96.70	99.26	96.33	97.43
PZ-SRC (ℓ_1)	97.07	98.53	95.97	97.19
PZ-C (ℓ_2)	95.60	97.06	95.60	96.09

$$\Omega_k \triangleq 100\left(\frac{\text{TP}_k}{273}\right) \tag{24}$$

where TP_k are the true positives of the target class k, for $k = 1, \ldots, K$, and the overall performance is defined as

$$\Omega \triangleq \frac{1}{K}\sum_{k=1}^{K} \Omega_k. \tag{25}$$

Note, both Ω and Ω_k quantify performance in percentages. For PZ moments, we consider $n = 10$ as the degree of the polynomials, which generates $P = 121$ PZ moments. In comparison to N, this is a dimensionality reduction by a factor of over 70. Note, the value of n can impact the performance of classification. Generally, higher values of n can represent an image better. However, very large values can cause numerical instabilities. Therefore, we select a moderate value of n. Few tests on the training data can also give a good idea over the choice of n. For sparse reconstruction, we use IHT for PZ-SRC (as well as for SRC and R_ω-SRC, for a fair comparison) and consider the order of sparsity $\Gamma = 5$. Note, the parameter Γ is a tuning parameter and can be selected based on different cross-validation approaches.

In terms of experimental results, we first consider the magnitude-only radar signatures. Table I shows the classification performance results of different classifiers. Note,

we also consider PZ moments based LSVC (PZ-LSVC) for the sake of comparison. We can see that SRC outperforms LSVC for all target classes. PZ-LSVC is slightly better than SRC in the overall performance, which shows that the usage of PZ moments improves the performance of a classifier, in general. We also provide the performance results of random projections based SRC, i.e., R_ω-SRC for $\omega = 05$, 15, and 35. As mentioned in Section III, the increasing value of ω causes a reduction in the computational complexity of the SRC. However, we can see from Table I that it also causes a proportional reduction in the classification performance. In comparison, PZ-SRC shows better classification performance than that of all the classifiers, in every category. Note, despite showing improved performance, the computational complexity of PZ-SRC is much less than that of other methods. In the current setting, the computational complexity of PZ-SRC is less than that of R_{70}-SRC, whereas its performance is significantly higher than that of R_{35}-SRC. Thus, we can say that in comparison with other methods, PZ-SRC provides significantly higher classification performance at a significantly lower computational complexity. We also compare the performance of PZ-SRC with reconstruction approaches different from (18). In (18), we use an ℓ_0-norm penalty to obtain a sparse solution. Since solving an ℓ_0-norm problem is NP-hard, we have used the IHT algorithm, which is a greedy algorithm, to approximate its solution. Another popular way to solve an ℓ_0-norm problem is to relax it by an ℓ_1-norm, which is also known as basis pursuit [7] or least absolute shrinkage and selection operator [29]. We denote PZ-SRC with ℓ_1-norm-based solver as PZ-SRC (ℓ_1). From Table I, we can see that the difference in performance between PZ-SRC and PZ-SRC (ℓ_1) is not significant. However, in our experiments, we observed that the former converged by an order of magnitude is faster than the latter. Apart from an ℓ_1-norm based reconstruction, we also compare the performance of PZ-SRC with ℓ_2-norm based reconstruction approach. This is known as Tikhonov regularization. We denote it by PZ-C (ℓ_2). As explained in Section IV, our OP is an underdetermined problem. In principle, an ℓ_2-norm based approach can solve such an OP. However, our OP also requires a sparse solution that cannot be achieved by an ℓ_2-norm based approach. Therefore, we can see from Table I that PZ-SRC outperforms PZ-C (ℓ_2).

Now, in the light of Section IV-C, we evaluate the performance of complex radar signatures for varying values of α (magnitude fraction) and β (phase fraction). Fig. 2 presents these performance results. We can see, in comparison to 97.43% of the magnitude-only signatures in Table I, that using complex signatures can enhance the performance of PZ-SRC to 99.14%, for $\alpha, \beta = 0.1$. In this paper, for the sake of simplicity, we keep $\alpha, \beta = 0.5$ for which $\Omega = 98.41\%$. For the rest of the experiments, we use fused complex signatures. We first obtain classification results by considering AuxFix discussed in Section IV-B1 as auxiliary atoms. Table II shows the confusion matrix in this regard. The performance improvement has been encouraging, with $\Omega = 98.53\%$. Next, we simulate the classification problem by considering AuxMov discussed in Section IV-B2 as auxiliary atoms. Table III shows the performance of PZ-SRC for varying sizes of W_k (same $\forall k$). We can see that the classification performance is affected by changing size of W_k. The best performance is achieved when W_k/J_k is a multiple of 0.5. If all the test measurements are divided into four quadrants, with each quadrant corresponding to a range of aspect angles of approximately 90°, then $W_k/J_k = 0.5$ essentially corresponds to the numerical size of one quadrant, when the best performance is achieved. This can be explained as follows. Due to the rotational invariance properties of the PZ moments, measurements at consecutive aspect angles are correlated with each other, in general, with some variations mostly because of radar reflectivity irregularities. However, measurements at the boundary of two quadrants correspond to the fine corners of the considered rectangular-shaped targets, and these measurements are highly uncorrelated with all the measurements in the preceding or the succeeding quadrant. This phenomenon can be seen in Fig. 3, which shows the correlations of a few training measurements (PZ moments) with the rest of the measurements in a kth target class. We can see that mutual correlations are minimum at quadrants, i.e., when $W_k/2 = 75$, 150, and 225. Thus, it is better to exploit only the correlated measurements for generating auxiliary atoms and that happens when the size of W_k is such that it contains most of the correlated measurements of a quadrant or its multiple. Since, correlation is an important parameter for generating auxiliary atoms, we next assess the classification performance by considering AuxCorr discussed in Section IV-B3. Table IV shows the classification performance with varying Υ. We can see that the best performance

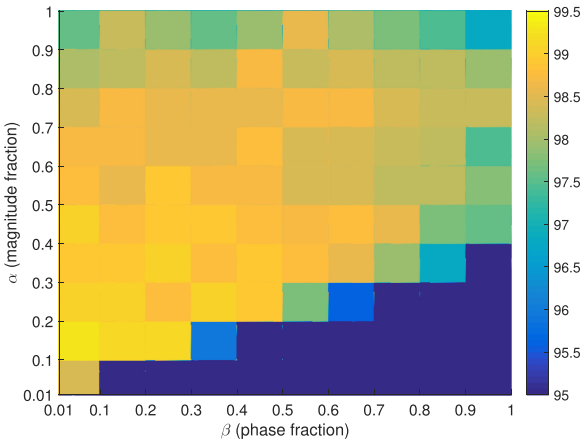

Fig. 2. Ω(%) for PZ-SRC (complex).

TABLE II
Confusion Matrix for PZ-SRC (AuxFix)

	2S1	D-7	T62	$\Omega_k(\%)$	$\Omega(\%)$
2S1	264	0	9	96.70	-
D-7	0	271	2	99.26	-
T62	0	1	272	99.63	-
	-	-	-	-	98.53

TABLE III
Performance With Varying W_k in (21)

W_k	29	59	89	119	149	179	209	239	269	299	328	358	388	418	448
W_k/J_k	0.1	0.2	0.3	0.4	0.5	0.6	0.7	0.8	0.9	1.0	1.1	1.2	1.3	1.4	1.5
$\Omega(\%)$	98.16	98.41	98.65	98.77	98.90	98.65	98.65	98.77	98.90	98.90	98.90	98.77	98.65	98.77	98.90

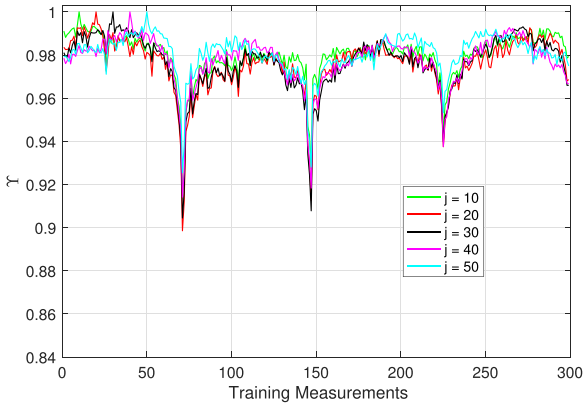

Fig. 3. Correlations among PZ-moments based measurements.

TABLE IV
Performance With Varying Υ in (23)

Υ	0.98	0.97	0.96	0.95	0.94	0.93	0.92
$\Omega(\%)$	98.29	98.53	98.65	98.77	98.90	98.53	98.53

TABLE V
Confusion Matrix for PZ-SRC (AuxMov)

	2S1	D-7	T62	$\Omega_k(\%)$	$\Omega(\%)$
2S1	266	0	7	97.43	-
D-7	0	271	2	99.26	-
T62	0	0	273	100	-
	-	-	-	-	98.90

TABLE VI
Comparison of Computation Time

	SRC	PZ-SRC	R_{05}-SRC	R_{35}-SRC
Time (sec)	111	4.23	20	5.5
$\Omega(\%)$	96.09	98.90	95.24	93.28

TABLE VII
PZ-SRC Versus PZ-C (ℓ_2)

	Magnitude Only $\Omega(\%)$	Complex $\Omega(\%)$	AuxCorr $\Omega(\%)$
PZ-C (ℓ_2)	96.09	95.72	94.87
PZ-SRC	97.43	98.41	98.90

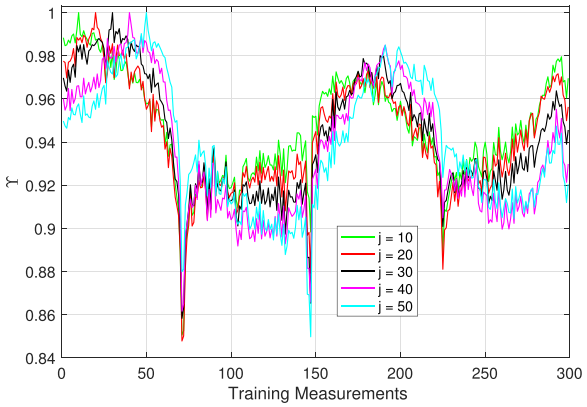

Fig. 4. Correlations among test measurements.

is achieved for $\Upsilon = 0.94$. This is quite understandable. A higher value of Υ does not collect enough number of informative measurements and a lower value of Υ involves noisy or noninformative measurements. This can be seen in Fig. 3 as well. We also provide a confusion matrix regarding the performance of PZ-SRC with fused complex signatures and using $W_k/J_k = 0.5$, in Table V. An overall performance of 98.90% is achieved. Note, the overall performance can reach over 99.50% for $\alpha, \beta = 0.1$ (see Section IV-C). This enhanced classification performance has been achieved at a very low computational cost. In our case, the computational complexity of PZ-SRC with a maximum number of J auxiliary atoms is less than R_{35}-SRC, whereas its classification performance is over 5% higher than R_{35}-SRC (see Table I). A comparison of computation time, using a Macbook Pro (2.2-GHz Intel Core i7, 16-GB 1600 MHz DDR3), is given in Table VI. We also compare the performance of PZ-C (ℓ_2) with our proposed methods of PZ-SRC. Table VII shows this comparison for magnitude-only measurements, complex measurements and when using auxiliary atoms from AuxCorr discussed in Section IV-B3. We can see that the holistic approach of PZ-C (ℓ_2) is not able to cope with the proposed modifications. However, the sparsity-preserving approach of PZ-SRC exhibits substantial gains and can perform more than 4% higher than PZ-C (ℓ_2), for a similar setting.

Note, in order to better appreciate the invariance properties of the PZ moments, we also plot the correlations among original test measurements, i.e., without PZ moments, in Fig. 4. We can see that the correlation structure is quite inconsistent in comparison to the PZ moments, as shown in Fig. 3.

VI. CONCLUSION

In this paper, we presented sparse representations for radar image classification by using PZ moments. We obtained a reduction in the dimensionality of the problem without compromising the performance. We exploited the invariance properties of the PZ moments to generate auxiliary atoms to complement the dictionary, which resulted in an enhanced classification performance. We used a fusion strategy to gain both from the magnitude and the phase of the radar signatures. We proved the validity of our proposed methods via numerical experiments on the MSTAR dataset.

ACKNOWLEDGMENT

This work has been approved for submission by TASSC-PATHCAD Sponsor, C. Holmes, Senior Manager Research, Research Department, Jaguar Land Rover, Coventry, U.K.

SHAHZAD GISHKORI, *Member, IEEE*
BERNARD MULGREW, *Fellow, IEEE*
University of Edinburgh, Edinburgh, U.K.

REFERENCES

[1] W. Carrara, R. Goodman, and R. Majewski
Spotlight Synthetic Aperture Radar. Boston, MA, USA: Artech House, 1995.

[2] S. Palm, R. Sommer, M. Caris, N. Pohl, A. Tessmann, and U. Stilla
Ultra-high resolution SAR in lower terahertz domain for applications in mobile mapping,
In *Proc. German Microw. Conf.*, Mar. 2016, pp. 205–208.

[3] K. El-Darymli, E. W. Gill, P. Mcguire, D. Power, and C. Moloney
Automatic target recognition in synthetic aperture radar imagery: A state-of-the-art review
IEEE Access, vol. 4, pp. 6014–6058, 2016.

[4] G. J. Owirka, S. M. Verbout, and L. M. Novak
Template-based SAR ATR performance using different image enhancement techniques
Proc. SPIE, vol. 3721, pp. 302–319, 1999.

[5] Q. Zhao and J. C. Principe
Support vector machines for SAR automatic target recognition
IEEE Trans. Aerosp. Electron. Syst., vol. 37, no. 2, pp. 643–654, Apr. 2001.

[6] B. Olshausen and D. Field
Emergence of simple-cell receptive field properties by learning a sparse code for natural images
Nature, vol. 381, pp. 607–609, 1996.

[7] S. S. Chen, D. L. Donoho, and M. A. Saunders
Atomic decomposition by basis pursuit
SIAM J. Sci. Comput., vol. 20, pp. 33–61, 1998.

[8] M. Aharon, M. Elad, and A. Bruckstein
K-SVD: An algorithm for designing overcomplete dictionaries for sparse representation
IEEE Trans. Signal Process., vol. 54, no. 11, pp. 4311–4322, Nov. 2006.

[9] K. Huang and S. Aviyente
Sparse representation for signal classification,
In *Proc. 19th Int. Conf. Adv. Neural Inf. Process. Syst*. Cambridge, MA, USA: MIT Press, 2006, pp. 609–616.

[10] J. Wright, A. Y. Yang, A. Ganesh, S. S. Sastry, and Y. Ma
Robust face recognition via sparse representation
IEEE Trans. Pattern Anal. Mach. Intell., vol. 31, no. 2, pp. 210–227, Feb. 2009.

[11] J. J. Thiagarajan, K. N. Ramamurthy, P. Knee, A. Spanias, and V. Berisha
Sparse representations for automatic target classification in SAR images,
In *Proc. 4th Int. Symp. Commun., Control, Signal Process.*, Mar. 2010, pp. 1–4.

[12] M. B. Wakin, D. L. Donoho, H. Choi, and R. G. Baraniukr
The multiscale structure of non-differentiable image manifolds,
In *Proc. SPIE*, pp. 413–429, 2005.

[13] S. T. Roweis and L. K. Saul
Nonlinear dimensionality reduction by locally linear embedding
Science, vol. 290, pp. 2323–2326, 2000.

[14] M. Yang, L. Zhang, J. Yang, and D. Zhang
Metaface learning for sparse representation based face recognition,
In *Proc. IEEE Int. Conf. Image Process.*, Sep. 2010, pp. 1601–1604.

[15] I. Ramirez, P. Sprechmann, and G. Sapiro
Classification and clustering via dictionary learning with structured incoherence and shared features,
In *Proc. IEEE Comput. Soc. Conf. Comput. Vis. Pattern Recognit.*, Jun. 2010, pp. 3501–3508.

[16] M. Yang, L. Zhang, X. Feng, and D. Zhang
Fisher discrimination dictionary learning for sparse representation,
In *Proc. Int. Conf. Comput. Vis.*, Nov. 2011, pp. 543–550.

[17] Y. Gao, J. Ma, and A. L. Yuille
Semi-supervised sparse representation based classification for face recognition with insufficient labeled samples,
IEEE Trans. Image Process., vol. 26, no. 5, pp. 2545–2560, May 2017.

[18] J. Lu, G. Wang, and J. Zhou
Simultaneous feature and dictionary learning for image set based face recognition
IEEE Trans. Image Process., vol. 26, no. 8, pp. 4042–4054, Aug. 2017.

[19] M.-K. Hu
Visual pattern recognition by moment invariants
IRE Trans. Inf. Theory, vol. 8, no. 2, pp. 179–187, Feb. 1962.

[20] F. A. Sadjadi and E. L. Hall
Three-dimensional moment invariants
IEEE Trans. Pattern Anal. Mach. Intell., vol. PAMI-2, no. 2, pp. 127–136, Feb. 1980.

[21] C.-H. Teh and R. T. Chin
On image analysis by the methods of moments
IEEE Trans. Pattern Anal. Mach. Intell., vol. 10, no. 4, pp. 496–513, Jul. 1988.

[22] A. Khotanzad and Y. H. Hong
Invariant image recognition by Zernike moments,
IEEE Trans. Pattern Anal. Mach. Intell, vol. 12, no. 5, pp. 489–497, May 1990.

[23] C. Clemente, L. Pallotta, I. Proudler, A. D. Maio, J. J. Soraghan, and A. Farina
Pseudo-Zernike-based multi-pass automatic target recognition from multi-channel synthetic aperture radar
IET Radar, Sonar, Navig., vol. 9, no. 4, pp. 457–466, 2015.

[24] C. Clemente, L. Pallotta, A. D. Maio, J. J. Soraghan, and A. Farina
A novel algorithm for radar classification based on Doppler characteristics exploiting orthogonal pseudo-Zernike polynomials
IEEE Trans. Aerosp. Electron. Syst., vol. 51, no. 1, pp. 417–430, Jan. 2015.

[25] F. Sadjadi
Comparative image fusion analysis,
In *Proc. IEEE Comput. Soc. Conf. Comput. Vis. Pattern Recognit. Workshops*, Jun. 2005.

[26] F. Sadjadi
Adaptive object classification using complex SAR signatures,
In *Proc. IEEE Conf. Comput. Vis. Pattern Recognit. Workshops*, Jun. 2016, pp. 299–303.

[27] T. Blumensath and M. E. Davies
Iterative hard thresholding for compressed sensing
Appl. Comput. Harmon. Anal., vol. 27, no. 3, pp. 265–274, 2009.

[28] E. R. Keydel, S. W. Lee, and J. T. Moore
MSTAR extended operating conditions: A tutorial
Proc. SPIE, vol. 2757, pp. 228–242, 1996.

[29] R. Tibshirani
Regression shrinkage and selection via the LASSO
J. Roy. Statist. Soc., Ser. B, vol. 58, pp. 267–288, 1994.